Modeling Electrochemical Migration of Sn-9Zn: Insights from Finite Difference and Finite Element Methods

Ali Dayoub[1)], Ali Gharaibeh[1)], Balázs Illés[1)], Bálint Medgyes[1)]

1) Department of Electronics Technology, Faculty of Electrical Engineering and Informatics, Budapest University of Technology and Economics, Műegyetem rkp. 3., H- 1111 Budapest, Hungary,

ali.dayoub@edu.bme.hu

Abstract—Electrochemical migration (ECM) is a significant reliability concern in electronic systems, occurring when moisture is present on conductor-dielectric-conductor structures under an applied bias voltage. The process involves three primary stages: metal dissolution at the anode, ion migration through the electrolyte under the influence of an electric field, and metal deposition at the cathode, leading to the formation of conductive dendrites. These dendrites grow over time, reducing surface insulation resistance and potentially causing failure by bridging the electrodes. This study examines ion transport modeled by the Nernst-Planck equation to simulate the ECM of Sn-9Zn in deionized (DI) water under applied voltages of 3V and 5V. The finite difference method (FDM) is used for simulation, and the results are compared with previously obtained data from the finite element method (FEM). The comparison revealed that both methods could predict similar electrochemical behaviors of Sn and Zn ion transport across the gap. However, differences were noted: At 3V, FDM simulations indicated a delayed dominance of Sn ion transport compared to Zn. FDM consistently computed lower concentration values for Both ions during the transport along the gap distance at both voltage levels. These findings emphasize the importance of carefully selecting and validating numerical methods when modeling the electrochemical behavior of specific metals and alloys.

Keywords—Electrochemical Migration, Finite Difference Method, Finite Element Method, Numerical Modeling

I. INTRODUCTION

Electrochemical migration (ECM) is a major reliability concern in microelectronic devices and circuits, particularly in humid environments. This phenomenon has been extensively studied due to its impact on the longevity and functionality of electronic components, especially in harsh environments. It occurs when metallic ions dissolve at the anode under a biased voltage, transport ions through an electrolyte, and are electrochemically reduced at the cathode, leading to the formation of metallic dendritic structures. These dendrites, often composed of metals such as copper, tin, or silver, can bridge the gap between conductive traces. As these dendrites grow, they lower surface insulation resistance, which can eventually cause

electrical short circuits and device failure. The issue is further intensified by the ongoing miniaturization of electronic devices, as higher electric field strengths and narrower conductor spacing increase the risk of ECM [1].

Sn-9Zn solder alloys have emerged as viable lead-free alternatives due to their excellent mechanical properties, cost-effectiveness, and relatively low melting point, comparable to conventional Sn-Pb solder alloys [2][3]. However, their susceptibility to ECM in humid environments presents a significant reliability challenge [4][5]. Since the addition of Zn in Sn solder has been found to slow down or prevent the growth of Sn whiskers [6], Sn-xZn solders have significant potential for use in the lead-free soldering industry. Research indicates that the development and morphology of dendrites during ECM are influenced by factors such as applied voltage, electrolyte characteristics, and the transport behavior of metallic ions. Specifically, the dissolution, migration, and reduction of Sn and Zn ions are governed by parameters like diffusion coefficients, ionic mobility, and anodic surface concentrations [7].

Numerical modeling plays a vital role in ECM research by enabling the simulation of ion transport mechanisms under controlled conditions [8]. The Nernst-Planck equation, which incorporates diffusion, migration, and advection, is commonly used to describe the transport of Sn and Zn ions [9][10]. Finite Element Method (FEM) simulations are widely employed to solve this equation in ECM studies, offering detailed predictions of ion concentration distribution and dendrite formation over time and space [11]. For instance, Ma et al. used FEM simulations in Elmer software to accurately model the transport behavior of Sn and Zn ions at 3V and 5V, revealing significant differences in ion dynamics at different voltage levels [12].

The Finite Difference Method (FDM) is a simple and computationally efficient numerical technique [10]. Although it is widely used for solving partial differential equations (PDE), its application in ECM studies has been relatively underexplored. However, recent work has confirmed its effectiveness, demonstrating its validity and potential for such applications [9][10]. This study aims to fill that gap by applying FDM to model ECM in Sn-9Zn alloys under conditions similar to those in [12], allowing for a direct comparison between the two methods.

This study primarily aims to evaluate the ability of FDM to model the transport kinetics of Sn and Zn ions during ECM and compare its results with those derived from FEM. By investigating differences in ion concentration profiles, the timing of dominance during the transport, and overall patterns, the research seeks to provide valuable insights into the strengths and limitations of both methods for ECM modeling. These insights are crucial for guiding future research and ensuring the reliability of lead-free solder alloys in electronic applications.

II. Materials and Methods

A. ECM behavior of Sn and Zn

This research investigates the ECM behavior of Sn-9Zn solder alloys in a deionized (DI) water-electrolyte. The Sn-9Zn alloy consists of 91.0 wt.% tin and 9.0 wt.% zinc, making it a widely studied lead-free solder material [12]. Based on the classical ECM model, both Sn and Zn undergo anodic dissolution, resulting in the formation of Sn^{2+} and Zn^{2+} ions, respectively, which can migrate and reduce at the cathode. A schematic representation of the ECM process for the Sn-9Zn solder alloy is shown in Fig. 1.

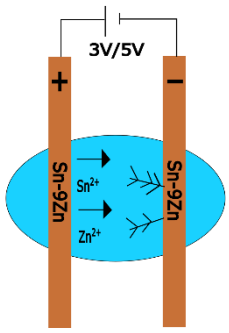

Fig. 1. ECM process diagram for Sn-9Zn electrodes

B. Key Distinctions: Comparing the Current and Previous Manuscript

This manuscript applies the FDM to replicate a previous numerical solution of the Nernst-Planck equation, which modeled the ion transport of Sn^{2+} and Zn^{2+} along the gap distance using the FEM [12]. However, several differences exist between the two approaches. One key difference lies in the applied boundary conditions: the previous study [12] used a Dirichlet condition for the ionic concentration and a Neumann condition for the potential, whereas the current study employs Dirichlet conditions for both. Additionally, the previous research [12] utilized a triangular mesh for the grid and solved the numerical system using Elmer software, while the present study adopts a rectangular grid and implements the solution in Python.

III. Methodology of Numerical Modeling

A. Governing Equations

In the region where ion transport occurs, the potential distribution can be found by applying Poisson's equation for electrostatics. However, due to the assumption of electroneutrality in the electrolyte, the net charge density (ρ) is effectively zero, which simplifies Poisson's equation to Laplace's equation [9]. Consequently, the potential distribution and electric field between the electrodes can be determined using the equations (1) and (2), respectively.

$$\nabla^2\varphi = \frac{\partial^2\varphi}{\partial x^2} + \frac{\partial^2\varphi}{\partial y^2} = 0 \qquad (1)$$

$$\bar{E} = -\nabla\varphi = -(\frac{\partial\varphi}{\partial x}, \frac{\partial\varphi}{\partial y}) \qquad (2)$$

When considering ion transport in the Sn-9Zn alloy, the impact of electroconvection on the overall transport within the ECM process on printed circuit boards (PCBs) is minimal [13]. As a result, metal cations produced at the anode—mainly Sn^{2+} or Zn^{2+} ions—transport through the electrolyte toward the cathode in response to the electric field lines. The ion transport is governed by the Nernst-Planck equation (Eq. 3), which takes into account both diffusion and migration. Diffusion causes ions to move from regions of higher concentration to lower concentration, while migration forces ions to move in the direction of the electric field.

$$\bar{J} = -D\nabla c - \mu c\nabla\varphi \qquad (3)$$

Here, J represents the mass flux of the metal cations, D is the diffusion coefficient of the respective ion (Sn^{2+} or Zn^{2+}), and c is the ion concentration. The ionic mobility μ of metal ions in the DI electrolyte is given by the following equation:

$$\mu = \frac{q\ F\ D}{R\ T} \qquad (4)$$

Where q is the ion charge number, F is the Faraday constant, R is the Universal Gas Constant, and T is the ambient temperature, respectively. In the absence of homogeneous reactions, the changes in the concentration of metal ions within the electrolyte droplet over time can be described using the continuity equation (Eq. 5), which allows for the calculation of ion concentrations in the grid as shown in Eq. (6).

$$\frac{\partial c}{\partial t} = -\nabla.J \qquad (5)$$

$$\frac{\partial c}{\partial t} = D\nabla^2 c + \mu\nabla c.\nabla\varphi \qquad (6)$$

B. Initial Conditions and Boundary Conditions

In the current computational ECM model, Dirichlet boundary conditions are applied to the electric potential and the concentrations of Sn^{2+} and Zn^{2+}, as detailed in Table 1 and Table 2, respectively. Additionally, the constants and physical parameters for both ions are provided in Table 3. To account for the anodic dissolution step, the surface concentration of Sn^{2+} at the anode is approximately 5.5 times higher than that of Zn^{2+} at both voltage levels, as reported in [12]. This is reasonable given that the Sn content in the Sn-9Zn alloy is nearly ten times greater than the Zn content.

TABLE I. LIST OF INITIAL CONDITIONS AND BOUNDARY CONDITIONS USED IN THE COMPUTATIONAL ECM MODEL FOR Sn^{2+}

Condition Type	**Location**	**ϕ [VDC]**	**Sn^{2+} ion concentration [mol/l]**

Initial Condition	***Anode***	3 / 5	7.5×10^{-6}/ 5.5×10^{-5}
	Cathode	0	0
Boundary Condition	***Anode***	3 / 5	7.5×10^{-6} / 5.5×10^{-5}
	Cathode	0	C_{cath-1}^{k-1}

TABLE II. LIST OF INITIAL CONDITIONS AND BOUNDARY CONDITIONS USED IN THE COMPUTATIONAL ECM MODEL FOR Zn^{2+}

Condition Type	**Location**	**ϕ [VDC]**	**Zn^{2+}ion concentration [mol/l]**
Initial Condition	***Anode***	3 / 5	1.34×10^{-6}/ 10×10^{-6}
	Cathode	0	0
Boundary Condition	***Anode***	3 / 5	1.34×10^{-6} / 10×10^{-6}
	Cathode	0	C_{cath-1}^{k-1}

TABLE III. PHYSICAL PARAMETERS OF Sn^{2+}AND Zn^{2+}

Parameter	**Value**	**Units**
F	96,500	C/mol
R	8.31	J/(mol K)
σ	0.024	S/m
T	298.0	K
$\mathbf{z_{Sn}}$	2	
$\mathbf{z_{Zn}}$	2	
$\mathbf{D_{Sn}}$	9.8×10^{-11}	m^2/s
$\mathbf{D_{Zn}}$	7.12×10^{-10}	m^2/s
$\mathbf{\mu_{Sn}}$	7.64×10^{-9}	$m^2/(V\cdot s)$
$\mathbf{\mu_{Zn}}$	5.55×10^{-8}	$m^2/(V\cdot s)$

C. *Grid Specification*

The electrochemical cell was modeled using a 2D rectangular computational grid with an equal number of points in both the x and y directions (nx = ny = 300). The grid was constructed with uniform spacing between each point in both directions (Δx = Δy = 1 micrometer). To ensure the numerical stability of the ECM computational model, the time step was determined by the Courant-Friedrichs-Lewy (CFL) condition [10], with a value of (500 μsec).

IV. Results and Discussion

A. *Ion Concentration Profiles*

The ion concentration profiles obtained using the FDM exhibit an exponential decay along the gap distance. In contrast, the FEM results reveal that, at both 3V and 5V, the Zn ion concentrations near the cathode closely match their concentrations at the anode [12].

Furthermore, a comparison of concentration values along the gap distance reveals that the ion concentrations calculated by FDM are consistently lower than those obtained using FEM. Notably, modeling the concentration profiles along the gap distance using FDM has never reached the anodic surface concentrations in any previous work, even over much longer periods, as illustrated in [9][10][13].

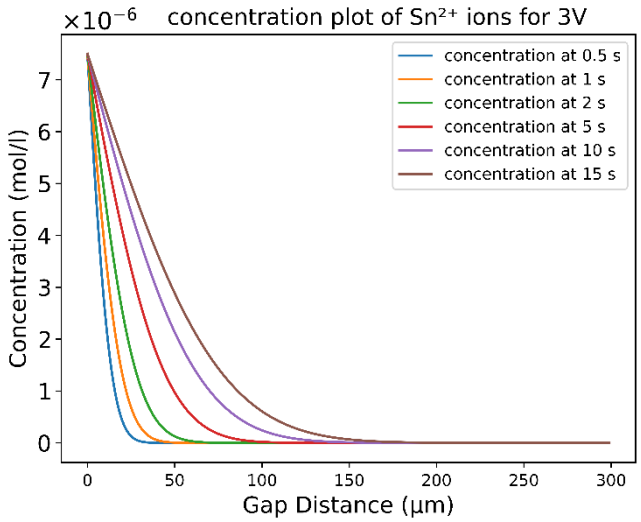

Fig. 2. Concentration profiles of Sn^{2+} ions at 3V as a function of the gap distance (with 0 μm representing the anode and 300 μm the cathode) for a constant surface concentration at the anode.

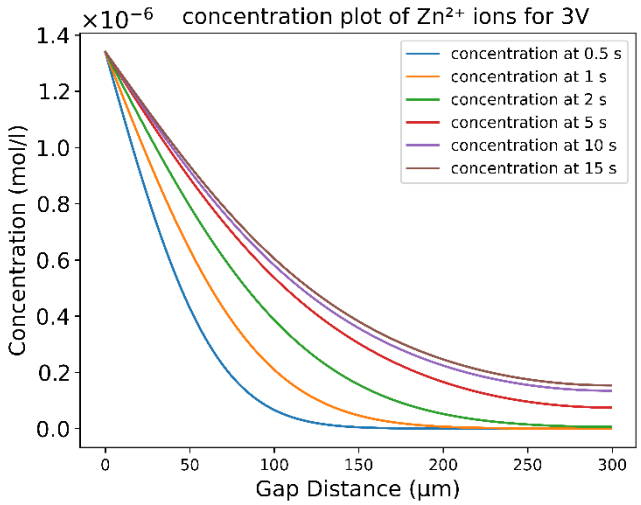

Fig. 3. Concentration profiles of Zn^{2+} ions at 3V as a function of the gap distance (with 0 µm representing the anode and 300 µm the cathode) for a constant surface concentration at the anode.

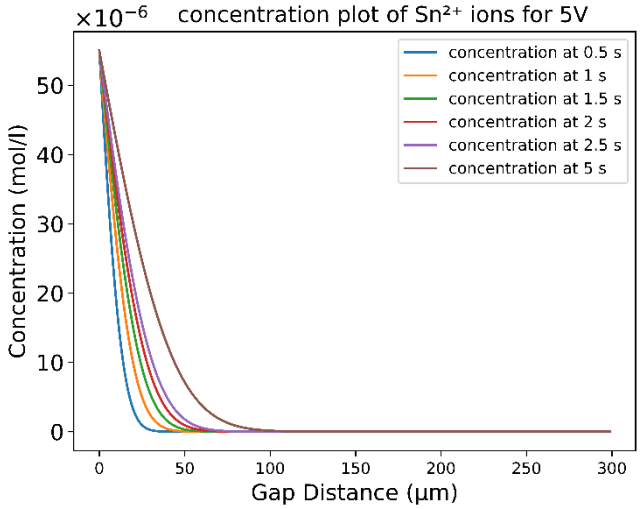

Fig. 4. Concentration profiles of Sn^{2+} ions at 5V as a function of the gap distance (with 0 µm representing the anode and 300 µm the cathode) for a constant surface concentration at the anode.

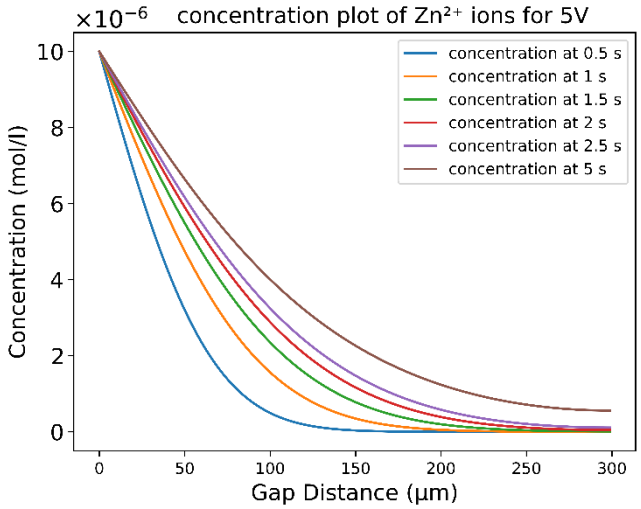

Fig. 5. Concentration profiles of Zn^{2+} ions at 5V as a function of the gap distance (with 0 μm representing the anode and 300 μm the cathode) for a constant surface concentration at the anode.

B. Timing of Ion Dominance

The timing of Sn^{2+} and Zn^{2+} ion dominance at the grid midpoint was examined under applied voltages of 3V and 5V, as illustrated in Fig. 6 and Fig. 7, respectively. At 3V, the FDM simulations indicated that Zn^{2+} ions initially dominated the midpoint before 27 seconds, after which Sn^{2+} ions became the dominant species. This behavior is similar to what has been reported using FEM. However, the transition to Sn^{2+} dominance occurred much earlier, around 10 seconds [12]. The initial dominance of Zn^{2+} at 3V is attributed to its higher mobility and diffusion coefficient compared to Sn^{2+}, allowing it to migrate more rapidly through the electrolyte. However, over time, the effect higher initial concentration of Sn^{2+} at the anode (5.5 times that of Zn^{2+}) led to its eventual dominance.

At 5V, Zn^{2+} remained dominant throughout the entire observation period. The primary reason for this sustained dominance is the greater mobility and diffusion coefficient of Zn^{2+} compared to Sn^{2+}, allowing Zn^{2+} ions to migrate faster and reach the cathode more efficiently. While FDM results showed that Zn^{2+} ions did not reach the anodic surface concentration of 1.0×10^{-5} mol/L within the observed time, FEM simulations [12] reported that Zn^{2+} reached this concentration in just 2 seconds. Additionally, in FDM, the highest concentration value at the midpoint of the grid at 5 seconds reached only 24% of the anodic surface concentration. These differences underscore the impact of numerical modeling choices on modeling ion migration. In the present case, FEM computes faster ion transport, particularly at higher voltages, while FDM tends to model the process as slower, leading to longer transition times for Sn^{2+} dominance at lower voltages.

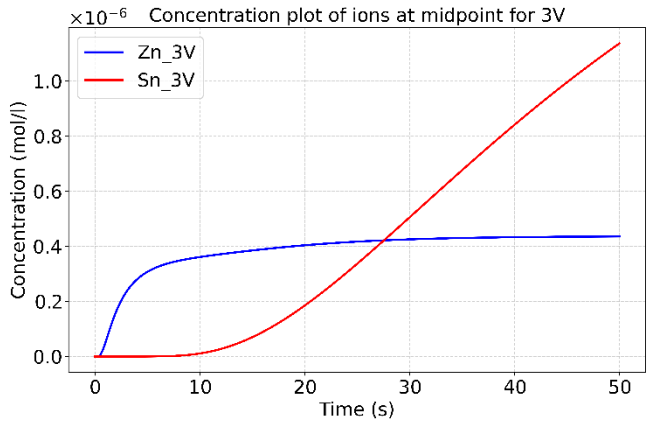

Fig. 6. Sn^{2+} and Zn^{2+} Ion Concentrations at the Midpoint at 3V.

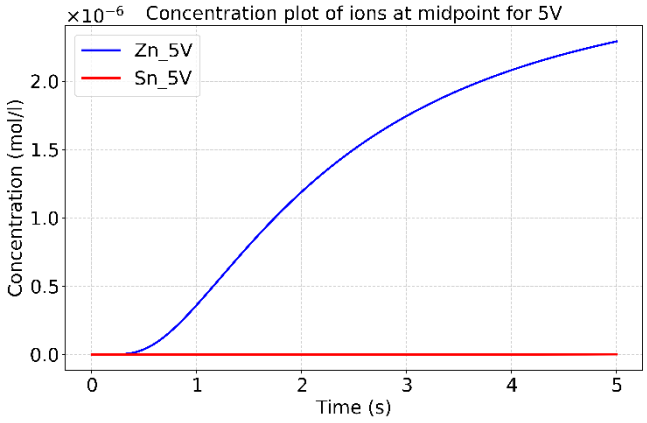

Fig. 7. Sn^{2+} and Zn^{2+} Ion Concentrations at the Midpoint at 5V.

C. *Overall Trends and Dendrite Formation*

Although there is no numerical modeling for dendrites in either the previous [12] or current work, if dendrite growth were simulated, the TTF would be shorter when using FEM, especially if the normalized concentration (c/c_{an}) across the grid was utilized to model the growth of dendrites as in [9][10].

Nevertheless, the pre-dendritic modeling helps explain why dendrites were Sn-rich at 3V and Zn-rich at 5V, as reported in the previous work [12] based on EDS analysis. However, the previous study relied on a single-spot EDS analysis for this explanation. Therefore, more comprehensive future research is needed to provide deeper insights into the migration mechanisms of Sn and Zn ions in Sn-xZn alloys.

Next to the numerical modeling illustrated above, it should be noted that from an experimental perspective, The significantly higher solubility product constant (K_{sp}) of $Zn(OH)_2$, at 1.2×10^{-17}, compared to that of $Sn(OH)_2$, at 1.0×10^{-28} [14][15], further enhances the migration rate of Zn ions along the gap distance. This is consistent with observations that the ECM rate of metals is strongly correlated with their K_{sp} values [13].

CONCLUSION

The current study compared the numerical solution of the Nernst-Planck equation using the FDM with results from the FEM to model ion transport in the ECM process of Sn-9Zn in DI water at applied voltages of 3V and 5V. A key distinction from previous work was the use of Dirichlet boundary conditions for both the electric potential and ion concentration, whereas prior FEM studies applied a Dirichlet condition for the ionic concentration and a Neumann condition for the electric potential. Additionally, the anodic surface concentration of Sn was assumed to be 5.5 times higher than that of Zn to account for the anodic dissolution step. The results demonstrated that both numerical methods computed similar trends in the transport of Sn^{2+} and Zn^{2+} ions along the gap distance in the DI droplet. However, differences were observed in the ion concentration profiles and transport rates. FDM consistently yielded lower concentration values than FEM and exhibited a delayed transition in ion dominance, particularly at 3V. Specifically, Sn^{2+} became dominant

later in FDM (27s) compared to FEM (10s), highlighting a slower diffusion of ions. At 5V, Zn^{2+} remained the dominant species throughout the simulation, aligning with expectations due to its higher mobility and diffusion coefficient. These findings emphasize the importance of numerical method selection in ECM modeling, as it significantly influences ion transport calculations and dendrite formation analysis.

These findings emphasize how the choice of numerical approach affects ECM modeling outcomes. The significant difference in the computed ion concentration profiles between the FEM and the FDM will further impact the modeling of dendrite growth, especially when normalized concentrations will be used. In particular, dendrite growth will occur more rapidly when using FEM, as the normalized concentrations are substantially higher.

ACKNOWLEDGMENT

The research discussed in this paper and carried out at BME has been supported by the National Research, Development and Innovation (NRDI) Office Fund based on the charter of bolster issued by the NRDI Office under the auspices of the Ministry for Innovation and Technology, and by the project FK 138220 and K 145966 of the NRDI Office.

REFERENCES

[1] E. L. Lee, Y. S. Goh, A. S. M. A. Haseeb, Y. H. Wong, M. F. M. Sabri, and B. Y. Low, "Review—Electrochemical Migration in Electronic Materials: Factors Affecting the Mechanism and Recent Strategies for Inhibition," *J. Electrochem. Soc.*, vol. 170, no. 2, p. 021505, Feb. 2023.

[2] L. Zhang *et al.*, "Development of Sn-Zn lead-free solders bearing alloying elements," *J. Mater. Sci. Mater. Electron.*, vol. 21, no. 1, pp. 1–15, Nov. 2010.

[3] J. C. Liu, Z. H. Wang, J. Y. Xie, J. S. Ma, G. Zhang, and K. Suganuma, "Understanding corrosion mechanism of Sn-Zn alloys in NaCl solution via corrosion products characterization," *Mater. Corros.*, vol. 67, no. 5, pp. 522–530, Oct. 2016.

[4] M. Y. Li, H. F. Yang, Z. H. Zhang, J. H. Gu, and S. H. Yang, "Fast formation and growth of high-density Sn whiskers in Mg/Sn-based solder/Mg joints by ultrasonic-assisted soldering: Phenomena, mechanism and prevention," *Sci. Rep.*, vol. 6, no. May, pp. 1–10, Jun. 2016.

[5] P. Xue, K. H. Wang, Q. Zhou, J. Huang, W. min Long, and Q. ke Zhang, "Effect of Nd on tin whisker growth in Sn–Zn soldered joint," *J. Mater. Sci. Mater. Electron.*, vol. 27, no. 4, pp. 3742–3747, Dec. 2016.

[6] C. C. Jain, C. L. Chen, H. J. Lai, and T. H. Chuang, "The inhibition of tin whiskers on the surface of Sn-8Zn-3Bi-0.5Ce solders," *J. Mater. Eng. Perform.*, vol. 20, no. 6, pp. 1043–1048, Mar. 2011.

[7] J. Y. Jung, S. B. Lee, H. Y. Lee, Y. C. Joo, and Y. B. Park, "Effect of ionization characteristics on electrochemical migration lifetimes of Sn-3.0Ag-0.5Cu solder in NaCl and Na 2SO 4 solutions," *J.*

Electron. Mater., vol. 37, no. 8, pp. 1111–1118, Aug. 2008.

[8] A. Gharaibeh, B. Illes, A. Geczy, and B. Medgyes, "Numerical Models of the Electrochemical Migration: A short review," *2020 IEEE 26th Int. Symp. Des. Technol. Electron. Packag. SIITME 2020 - Conf. Proc.*, pp. 178–183, 2020.

[9] B. Illés, B. Medgyes, K. Dušek, D. Bušek, A. Skwarek, and A. Géczy, "Numerical simulation of electrochemical migration of Cu based on the Nernst-Plank equation," *Int. J. Heat Mass Transf.*, vol. 184, p. 122268, Nov. 2022.

[10] A. Dayoub, A. Gharaibeh, B. Illés, and B. Medgyes, "Insights into copper electrochemical migration through numerical modeling and Monte Carlo simulation," *Results Eng.*, vol. 25, no. December 2024, 2025.

[11] A. Kunwar, H. Ma, J. Sun, S. Li, and J. Liu, "Modeling the diffusion-driven growth of a pre-existing gas bubble in molten tin," *Met. Mater. Int.*, vol. 21, no. 5, pp. 962–970, Nov. 2015.

[12] H. Ma *et al.*, "Study of electrochemical migration based transport kinetics of metal ions in Sn-9Zn alloy," *Microelectron. Reliab.*, vol. 83, no. May 2017, pp. 198–205, Feb. 2018.

[13] X. He, M. H. Azarian, and M. G. Pecht, "Analysis of the kinetics of electrochemical migration on printed circuit boards using Nernst-Planck transport equation," *Electrochim. Acta*, vol. 142, pp. 1–10, Jun. 2014.

[14] X. Zhong, L. Chen, B. Medgyes, Z. Zhang, S. Gao, and L. Jakab, "Electrochemical migration of Sn and Sn solder alloys: A review," *RSC Adv.*, vol. 7, no. 45, pp. 28186–28206, May 2017.

[15] D. Q. Yu, W. Jillek, and E. Schmitt, "Electrochemical migration of Sn-Pb and lead free solder alloys under distilled water," *J. Mater. Sci. Mater. Electron.*, vol. 17, no. 3, pp. 219–227, Nov. 2006.